Document history

Date	Action
1/Jul/2020	MS sent to co-authors for final draft acceptance
3/Jul/2020	IGSN for samples requested
	Spreadsheet and scripts submitted to Zenodo.
	MS Submitted to EarthArXiv
8/Jul/2020	Preprint DOI Received
	MS Submitted to Nature Geoscience
14/Jul/2020	IGSN received and inserted for all samples
	Small style adjustments to tables
21/Jul/2020	Received initial decision from Nature Geoscience
	Transferred to Nature Communications
29/Jul/2020	Sent to reviewers by Nature Communications

An Early Pliocene relative sea level record from Patagonia (Argentina)

Alessio Rovere[1*], **Marta Pappalardo**[2], **Sebastian Richiano**[3], **Marina Aguirre**[4], **Michael R. Sandstrom**[5], **Paul J. Hearty**[6], **Jacqueline Austermann**[5], **Ignacio Castellanos**[7], **and Maureen E. Raymo**[5]

[1]MARUM - Center for Marine Environmental Sciences, University of Bremen
[2]Department of Earth Sciences, Universitá degli studi di Pisa
[3]Instituto Patagónico de Geología y Paleontología, CONICET, Puerto Madryn
[4]CONICET, CCT-La Plata and Universidad Nacional de La Plata
[5]Lamont Doherty Earth Observatory, Columbia University
[6]Department of Geological Sciences, Jackson School of Geosciences, The University of Texas at Austin
[7]Baker Hughes

Abstract

We report ciao a geological unit surveyed and dated in central Patagonia, Argentina (Camarones town, San Jorge Gulf). The unit was interpreted as representative of an intertidal environment and dated to the Early Pliocene (4.69-5.23 Ma) with strontium isotope stratigraphy. The elevation of this unit was measured with differential GPS at ca. 36 m above present-day sea level. Considering modern tidal ranges, it was possible to constrain paleo relative sea level within ±2.5m (1σ). We use glacial isostatic adjustment models and estimates of vertical land movement to calculate that, when the Camarones intertidal sequence was deposited, global mean sea level was 28.4 ± 11.7m above present. This estimate matches those derived from analogous Early Pliocene sea level proxies in the Mediterranean Sea and South Africa. Evidence from these three locations indicates that Early Pliocene sea level may have exceeded 20m above its present level. Such high global mean sea level values imply an ice-free Greenland, a significant melting of West Antarctica, and a contribution of East Antarctica to global mean sea level.

***K*eywords** Early Pliocene · Sea level · Stratigraphy

1 Introduction

The survey, interpretation and dating of paleo relative sea sevel (RSL) indicators (such as fossil coral reefs or relic beach deposits[1]) is paramount to constraining the maximum elevation reached by global mean sea level during periods of the Earth's history warmer than the pre-industrial. Once measured, observed paleo RSL indicators must be corrected for processes causing *"Departures from Eustasy"*[2] (such as tectonics, mantle dynamic topography, DT, and glacial isostatic adjustment, GIA[3;4]) the elevation of paleo RSL indicators is the only direct proxy available to estimate global mean sea level in Earth's past. These estimates are in turn important to informing models of ice sheet melting under future warmer climates[5].

A recent global compilation by Khan et al., 2019[6] showed that more than 5000 RSL indicators globally span the last 30 ka. The number of surveyed RSL indicators is greatly reduced for older time periods: another compilation of Pleistocene RSL indicators[7] reports that more than 1000 Last Interglacial (MIS 5e, 125 ka) and only around 20 MIS 11 (400 ka) RSL indicators are preserved globally. Only a handful of sites exist that document sea level highstands beyond one million years ago[2;8;9;10]. In general, robust RSL indicators predating 400 ka are rare because they are poorly preserved and difficult to date with precision. Additionally, relating them to global mean sea level, GMSL, is difficult since they are likely affected by significant post-depositional movement. This limits our ability to gauge the sensitivity of ice caps to warmer climate conditions, such as those that characterized Earth in the Pliocene.

Some of the oldest, precisely dated and measured RSL indicators were recently surveyed on the island of Mallorca (Balearic Islands, Spain), in a coastal cave called *"Coves d'Artá"*. Here, six phreatic overgrowths on speleothems mark the paleo water/air interface within the cave[9], and are therefore closely related to paleo RSL. The highest and oldest of these formations was measured at 31.8 ± 0.25m above mean sea level, and yielded a U-Pb age of 4.29 ± 0.39Ma (2σ)[9]. Taking into account GIA and possible long-term deformation due to tectonics or dynamic topography, it was estimated that global mean sea level at the time of deposition of this RSL indicator was 25.1m above present, bounded by uncertainties represented by 16th-84th percentiles of 10.6-28.3m[9]. For the same time period, a second study[10] reported a site in the Republic of South Africa (Northern Cape Province, site Cliff Point, ZCP, Section2). Here, oyster shells living in a paleo subtidal to intertidal environment constrain paleo RSL at 35.1 ± 2.2 m (1σ). The oysters were dated to 4.28-4.87 Ma (2σ range) with strontium isotope stratigraphy (SIS). While paleo global mean sea level estimates were not calculated at this site, based on the Mallorca benchmark the authors argue that this location was affected by relatively minor vertical land movements (possibly uplift) since 5 Ma.

While indirect paleo sea level estimates spanning the last 5.3 Ma are available from oxygen isotopes[12;13], the two studies cited above are arguably the only ones reporting relatively precise and well-dated direct sea-level observations for the Early Pliocene. This period coincides with the Pliocene Climatic Optimum, that is regarded as a past analogue for future warmer climate[14]. At this time, CO_2 was between pre-industrial and modern levels[15] and, during interglacials, average global temperatures were 2-
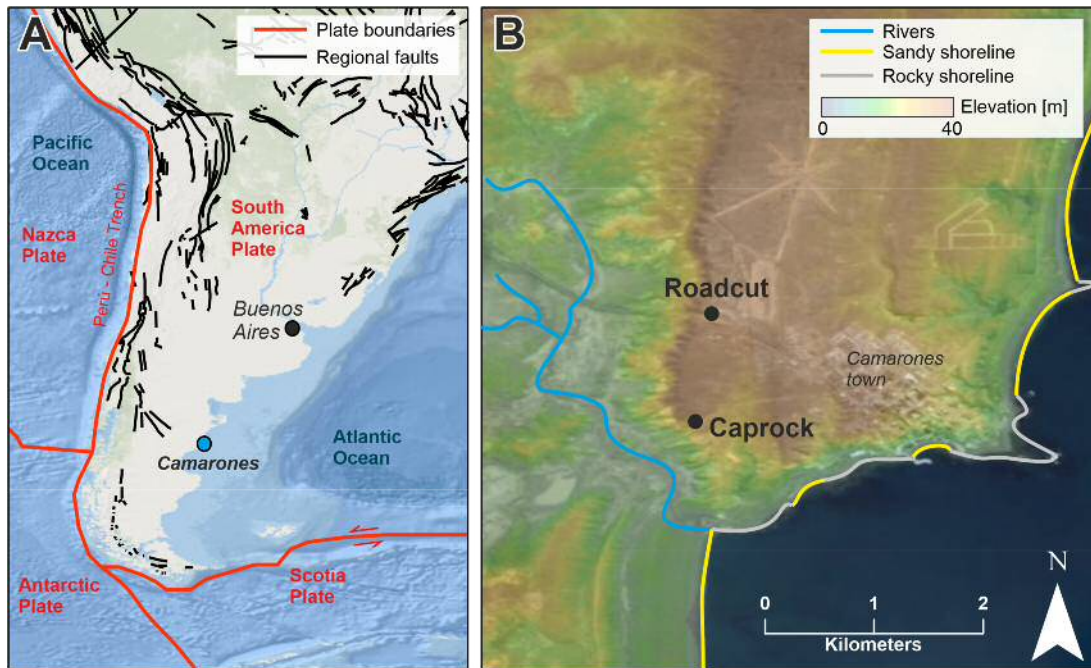
Figure 1: A) Location of the study area and main geological structures in the Southern part of South America. B) Topography of the Camarones town area, with location of the two outcrops (*Roadcut* and *Caprock*) presented in this study. Map sources: Esri, DigitalGlobe, GeoEye, Earthstar Geographics, CNES/Airbus DS, USDA, USGS, AeroGRID, IGN, DeLorme, GEBCO, NOAA NGDC, SRTM, the GIS User Community and other contributors. Elevation data in B are from the Shuttle Radar Topography Mission[11]

3°C higher than pre-industrial values[16]. Pliocene climate was modulated by a ca. 40kyr periodicity in glacial/interglacial cycles with highstands and lowstands that were characterized by sea-level oscillations as high as $13 \pm 5m$[17]. Ice models suggest that, during the warmest Pliocene interglacials, Greenland was ice-free[18]. The West Antarctic Ice sheet was subject to periodic collapses[19], contributing as much as 7m[20] to global mean sea level. Ice models and field-based evidence[21] suggest that also the East Antarctic Ice Sheet might have been smaller than today, contributing another 3m[20] to 13-16m[22] to global mean sea level.

In this study, we report an Early Pliocene foreshore (intertidal) sequence located in the town of Camarones, along the coast of central Patagonia, Argentina (fig. 2). Combining field data, SIS ages, GIA and DT models we conclude that this deposit formed 4.69-5.23Ma ago (2σ range) when sea level was 28.4 ± 11.7 (1σ) higher than today. This estimate is broadly consistent with those derived from the Republic of South Africa and Spain. Together, these three studies present a consistent picture of global mean sea level during the Pliocene Climatic Optimum that exceeded 20m above modern sea level.

The Pliocene sea level record at Camarones, Central Patagonia, Argentina

The Patagonia geographic region includes territories belonging to the states of Argentina and Chile. Geologically, Patagonia represents the southernmost tip of the South American plate (Figure 1A). Along the Pacific coasts of Patagonia, the Nazca and the Antarctic plates are subducting below the Andes. Towards the south, the Scotia plate moves eastward and outlines

Tierra del Fuego, at South America's southern tip[23]. To the East, the Patagonian Atlantic coast is a passive margin, tectonically characterized as an extensional stress field and bordered by a wide continental shelf. The central and eastern parts of this landmass are represented by the Andean foreland, formed by a Palaeozoic-Mesozoic metamorphic basement overlapped by Tertiary continental and marine sedimentary rocks, dating back to the Paleocene. These are covered by Eocene–Oligocene pyroclastic rocks and Middle Miocene fluvial sediments. Marine sedimentary rocks corresponding to Tertiary transgressions are located east of the Andean foreland[24]. In the Middle Miocene, the Chile Triple Junction migrated northward, leading to the opening of an asthenospheric window below southern Patagonia[25]. This caused a switch from subsidence to uplift, and the Patagonia region underwent a moderate but continuous uplift.[26]

Along the coastlines of Central Patagonia, several levels of paleo shorelines above modern sea level were already noted by Charles Darwin in his Beagle voyage[27], and were the subject of more than 150 years of research (see Supplementary Information for details). Studies in Central Patagonia include coastal sequences of Holocene[28;29], Pleistocene[30;31;32] and Pliocene-to-Miocene[33;34] age. Among the latter, Del Río et al[34] dated Early Pliocene mollusks from marine deposits few hundreds of kilometers south of the study area described in this study (see Supplementary Information for details).

The town of Camarones lies at the northern tip of the San Jorge Gulf, approximately 1300 km south of Buenos Aires, the capital of Argentina. Within a few kilometers of Camarones, several paleo-sea level indicators have been preserved, from the Holocene[35] to the Pleistocene[30]. Already in the late 1940s, the

Figure 2: The *Roadcut* outcrop at Camarones. The inset shows a detail of Unit **Cp**, a shelly-rich layer interpreted as representative of a foreshore (intertidal) environment dating to the Early Pliocene. Each unit is described in details in the Supplementary Information, including descriptions of the *Caprock* outcrop.

Italian geologist Feruglio[36] identified an elevated marine terrace along a roadcut carved on the main road leading into the town of Camarones that he tentatively attributed to the Pliocene. A recent study[30] confirmed the elevation of this terrace at ca. 40m above sea level, which is therefore located at the lower bound of the *"beach barries and terrace deposits between 40 and 110m elevation"* as reported in the 1:250.000 geological chart of Camarones[37].

Radiometric ages, precise GPS elevations and stratigraphic descriptions of cross-sections surveyed along this so-called High Terrace (originally named, in Spanish, *Teraza Alta de Camarones*[36]) are the subject of this paper. Along this terrace, we surveyed and dated samples from two sites, separated by less than one kilometer. One is the *Roadcut*, already recognized and described by Feruglio[36]. We did not find reports of the second site (that we here call *Caprock*, Figure 1B) in the existing literature, although it is possible that it was included in the geological description of the High Terrace by previous authors. At both sites, we recognized a geological facies representative of sedimentation in a foreshore environment (i.e. in the intertidal zone) that marks paleo RSL with high accuracy. All data described hereafter and in the Supplementary Information annexed to this article is available in a spreadsheet uploaded to Zenodo[38]

Paleo RSL. In general, *Roadcut* and *Caprock* represent sedimentation during a transgressive event on top of a raised shore platform (see Supplementary Information for details). Among the units identified within the *Roadcut* (Figure 2), one (Unit **Cp**, see inset in Figure 2) is composed of well-cemented fine conglomerates with rounded pebbles and shells. In particular, the uppermost part of this unit contains a dense faunal assemblage in the form of a shellbed, where we recognized 15 different

species of bivalves and 11 species of gastropods (see Supplementary Information for details). The bivalve shells are mostly intact and sometimes with paired valves (articulated), but not in living position. This unit was interpreted as representative of a foreshore environment, i.e. the intertidal zone. The same unit has been identified at the *Caprock* section, at roughly the same elevation. The elevation of Unit **Cp** was measured at two points at both *Roadcut* and *Caprock* (Table 1). From these measurements, we calculate that Unit **Cp** has an **average elevation of 36.2 ± 0.5m (1σ)** above the GEOIDEAR16 geoid[39], which approximates present sea level. Using modern tidal values[35], and assuming no post-depositional movement, we calculate that the two outcrops in the area of Camarones are indicative of a **paleo RSL at 36.2 ± 2.5m (1σ)** above present (see Methods for details).

Age. Three oyster shells from *Roadcut* and *Caprock* were analyzed by Strontium Isotope Stratigraphy (SIS) relative dating techniques. Using sequential leaching to target the least altered inner carbonate of each shell (Sandstrom et al., under review), we obtained multiple SIS ages on three different shells (one from *Caprock* and two from *Roadcut*). The shells yielded an age range of **4.69-5.23Ma** (n=6, 2σ S_{EM}) (see Methods and Supplementary Information for details).

Glacial Isostatic Adjustment. The Early Pliocene intertidal units surveyed at Camarones were subject to processes that caused their past and current elevation to depart from eustasy. These processes must be accounted for in order to reconstruct global mean sea level at the time of formation. We calculate Glacial Isostatic Adjustment (GIA) using 36 different Earth models. For this site, we calculate a GIA correction of −14.6 ± 3.2m (1σ) (see Methods for details). This value is subtracted from the

observed paleo RSL and the uncertainty propagated. This correction is a combination of effects associated with the ongoing response to the last deglaciation and Antarctic ice sheet oscillations during the early Pliocene[2]. The former contribution is -9.5 ± 3m (1σ), which means that the Argentinian coast today experiences sea level fall due to a combination of effects associated with postglacial rebound due to the melting of the glacial Patagonian ice sheet as well as continental levering, ocean syphoning, and rotational effects. Once fully relaxed, sea level at Camarones will therefore be lower (and a paleo sea level indicator higher) by approximately 9.5m than it is today. The additional contribution of ~ -5m is associated with the adjustment to 40kyr oscillations in the Antarctic ice sheet. The result is that, at Camarones, **GIA-corrected paleo RSL is 50.8 ± 4.1m (1σ)**.

Vertical Land Motions. The GIA-corrected RSL elevation reported above needs to be further corrected for Vertical Land Motions (VLMs), that can be either due to crustal tectonics, mantle dynamic topography[40;41] or deformation associated with sediment loading/unloading[42;43]. As briefly outlined in the previous sections, Camarones is located on a passive margin, likely subject to limited tectonic influence (see Supplementary Information for details). Dynamic topography models suggest that, since MIS 5e (125 ka), the area of Camarones was subject to uplift, with rates increasing towards the South[3]. This is in line with observations of much higher Pliocene shorelines (70-170m above sea level[34]) at locations 300-500 kilometers south of Camarones (see Supplementary Information for details). A long-term slight uplift trend is also predicted by the models of Flament et al., 2015[44] and Müller et al., 2018[45]. Predictions in these DT models average to 4.5 ± 2.2m/Ma (Table 3). Accounting for the age of the deposit, this leads to a downward correction of our global mean sea level inference by 22.5 ± 11.0m (1σ). As is apparent from the variation of estimates for the dynamic topography rate, this correction remains quite uncertain and the true value can possibly be even outside of this range given that it is difficult to fully explore model uncertainties.

Global Mean Sea Level. Using the value of VLM reported above and propagating the uncertainties related to RSL, GIA and VLM, we calculate that, at the time of deposition of the *Caprock* and *Roadcut* outcrops, **global mean sea level was 28.4 ± 11.7m (1σ)**. We remark that there are large unknowns associated with this value. First, as described above, dynamic topography remains to be a process that has high uncertainties that are generally not fully quantified. Second, it is possible that, as it is the case for the US Atlantic Coastal Plain[42], flexural response to sediment loading or tectonic deformation (that are not considered here) could also contribute to further vertical land motions in this area.

Early Pliocene Global Mean Sea Level

Until recently, field evidence to support the answer to the question *"How high was global mean sea level in the Early Pliocene?"* was elusive. A trilogy of independent lines of evidence is now available to answer this question. The age of the outcrops reported in this paper overlap with recently published data from Spain[9] and South Africa[10] (Figure 3A). The common denominator to these three sites is that they all report precise
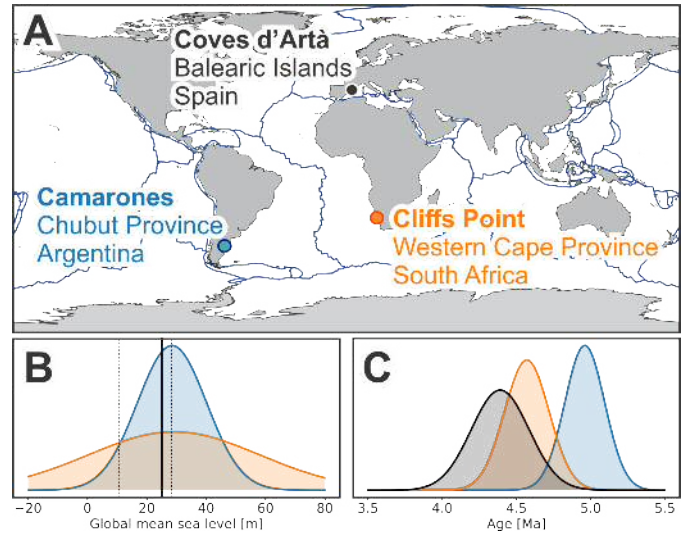

Figure 3: A) Location of Early Pliocene RSL indicators discussed in the text. Plate boundaries are shown in dark blue for reference. Background global map from GSHHS[46], plate boundaries from Bird, 2003[47]. B) Global Mean Sea Level (GMSL) estimates for: i) Coves d'Artá (Balearic Islands, Spain), solid black line represents 16th percentile (25.1m), dotted black lines the 16th-84 percentiles[9]; ii) Camarones (Chubut Province, Argentina), blue normal distribution as described here (28.4 ± 11.7m, 1σ); iii) Cliffs Point (Northern Cape Province, South Africa), orange normal distribution as calculated from data in Hearty et al., 2020[10], corrected with the same GIA and DT models used for Camarones (29.1 ± 29m,1σ). C) Age estimates for Coves d'Artá (black), Camarones (blue) and Cliffs Point (Orange). The python scripts to produce panels B and C is available via Zenodo[48].

and well-dated RSL indicators and have been subject to minor or mild uplift.

While uncertainties in the estimated vertical land motions necessarily lead to large uncertainties in the global mean sea level estimates, there is overlap between the calculated global mean sea levels for Camarones (28.4 ± 11.7m, 1σ) and Coves d'Artá (25.1m, with 16th-84th percentiles of 10.6-28.3m, Figure 3B).

An estimate of global mean sea level from the proxy record at Cliffs Point, South Africa[10] is characterized by greater uncertainty. Corrected with the same GIA models used for Camarones (Table 2), this data point indicates a paleo RSL at 44.7 ± 2.7m (1σ). The same DT models used at Camarones indicate possible uplift of 3.4 ± 6.3m/Ma (1σ). This results in an average global mean sea level estimate that aligns with that from Camarones, but bounded by very large uncertainties (Figure 3B).

Despite the relevant uncertainties, the average global mean sea level calculated from the geological facies reported in Argentina (this study), South Africa[10] and Spain[9] is well above modern sea level. In each area, post-depositional uplift contributes significant uncertainties to these estimates. We remark that, within each of these broader regions, there are other well-constrained Plio-Pleistocene sea level index points that may eventually provide a better calibration for modeled uplift rates.

The fact that locations on three continents and of comparable age give such similar estimates for paleo-RSL increases our confidence in stating that global mean sea level during the Pliocene Climatic Optimum likely exceeded 20m above present-day. This conclusion would most likely require an ice-free Greenland, a significantly melted West Antarctic Ice Sheet and a significant contribution from the East Antarctic Ice Sheet. These results can serve as an important calibration target for ice sheet modeling and, of even more obvious concern, imply that the polar ice sheets will not be immune to the impacts of ongoing global warming

METHODS

Elevation measurements and paleo RSL estimates. We measured elevations with a high-precision differential GPS system (Trimble ProXRT receiver and Trimble Tornado antenna) equipped to receive OmniSTAR HP real-time corrections. These corrections, in optimal conditions, allow to measure the elevation of a point with an accuracy of 0.1-0.6 m (2σ), depending on the survey conditions. We remark that, while at the *Caprock* outcrop there is a free view of the sky, at the *Roadcut* satellite reception is hindered by the vertical cliff face. This could explain, in part, the discrepancy in the two points collected at this outcrop at relatively short distance from each other. Data were originally recorded in geographic WGS84 coordinates and in height above the ITRF2008 ellipsoid. For each GPS point, we calculated heights above Mean Sea Level (orthometric height) subtracting from the measured ITRF2008 ellipsoid height the GEOIDEAR16 geoid height[39]. These geoidal elevations are the best available approximation of mean sea level in this area. GEOIDEAR16 was estimated to have an overall accuracy of 10 cm (https://www.ign.gob.ar/NuestrasActividades/Geodesia/Geoide-Ar16). The location and elevations of Unit **Cp** at *Roadcut* and *Caprock* are reported in Table 1. On average, we calculate that the elevation of Unit **Cp** is 36.2 ± 0.5m (1σ).

Table 1: GPS position and elevation of Unit **Cp** measured at the *Roadcut* and *Caprock* sites. Lat/Lon are in WGS84 coordinates, Ellipsoid heights are referred to the ITRF08 ellipsoid, geoid heights to the GEOIDEAR16 geoid model.

Longitude (dec.degrees E)	Latitude (dec.degrees N)	Ellipsoid Height (m)	Height above geoid (m)	Elev. error 1σ (m)
Roadcut				
-65.727604	-44.790083	49.67	36.8	0.06
-65.727619	-44.790069	47.68	34.8	0.3
Caprock				
-65.728221	-44.799297	49.40	36.5	0.2
-65.728221	-44.799298	49.64	36.8	0.1
			Average	**36.2**	**0.5**

The Unit **Cp** at the *Roadcut* and *Caprock* sites has been interpreted as forming in the foreshore zone, i.e., in the intertidal zone. This means that its indicative meaning[49] spans from Mean Lower Low Water (MLLW) to Mean Higher High Water

(MHHW). Based on predicted tidal data for the harbour of Camarones (link), Bini et al.[35] report that the maximum tidal range (MHHW to MLLW) in Camarones is 5m. Using this value and the formulas described in Rovere et al., 2016[1], we calculate that paleo RSL associated with Unit **Cp** is 36.2 ± 2.5m. We highlight that this value does not take into account the possibility that, 5 Ma ago, tidal ranges were different than present-day ones, due to different shelf bathymetry under higher sea levels[50].
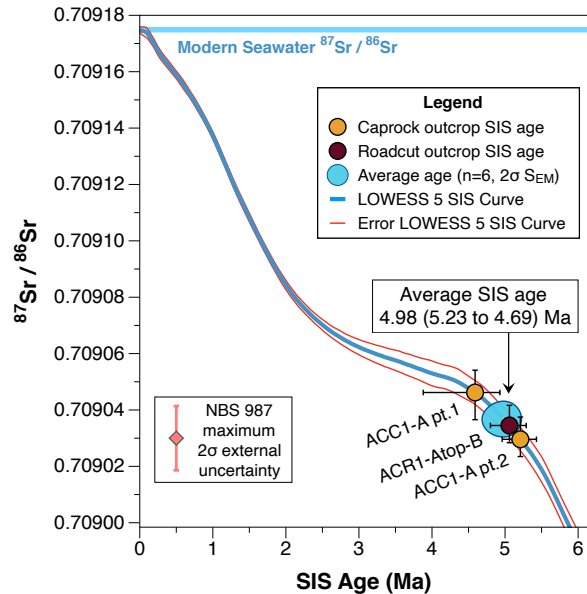

Figure 4: Sr isotope stratigraphy relative ages of oyster shells plotted on the SIS curve (LOWESS version 5)[51]. Orange points are from two separate portions of a shell from the *Caprock*, while maroon point is of a shell from unit **Cp** in the *Roadcut*. The average SIS age based on these samples is shown as a blue ellipse. Only inner leaches on the best-preserved specimens are shown. For the full dataset, see the Supplementary Information annexed to this paper. Modern seawater ^{87}Sr/^{86}Sr values shown in light blue line. Maximum 2σ external uncertainty for the Sr isotope external standard NBS 987 is shown as red point for comparison (see Methods for details).

Strontium Isotope Stratigraphy ages. To attribute an age to Unit **Cp**, we used the Strontium Isotope Stratigraphy (SIS) curve published by McArthur et al. (2012)[51] (LOWESS version 5). Sr isotope ratios from carbonates are susceptible to post-depositional alteration, therefore, any significant reworking of Sr isotopes needs to be detected and discarded. Information on shell preservation was determined using ^{87}Sr/^{86}Sr measurements on sequentially leached shell material (assuming smaller Sr isotope variations between leaches implies better preservation[52;53]) alongside standard screening techniques[34;54] and elemental analysis[55;56]). A preservation index between "1" (unaltered) and "3" (highly altered) was established for each sample based on these criteria (see Supplementary Information for details)with samples scoring above "2.0" excluded from results (see Hearty et al., 2020[10] and Sandstrom et al., under rev. for details).

We selected Ostreidae species for SIS chronological constraints, primarily because these shells precipitate original calcite mineral phases, making them more robust to diagenesis than arag-

onitic shells. Sample screening and chemical processing was carried out at Lamont Doherty Earth Observatory (LDEO), and all ^{87}Sr/^{86}Sr measurements were made using Thermal Ion Mass Spectrometry (TIMS) on an IsotopX Phoenix at SUNY Stonybrook University (SBU) or a Finnigan Triton Plus at Lamont Doherty Earth Observatory (LDEO).

We measured three oyster shells, one from the *Caprock* and two from the *Roadcut* unit. The *Caprock* oyster (ACC1-A) was sampled in three different locations, with inner leaches measured on two of those splits, returning SIS ages of 4.59Ma (3.88 to 4.93Ma) and 5.21Ma (4.96 to 5.44Ma) (Figure 4). The third sampling location was only measured for full dissolution, with an average SIS age of 4.65Ma (4.42 to 4.83Ma), but provided confidence in the shell Sr isotope heterogeneity and validated analytical uncertainties (see Supplementary Information for details). The preservation index score for the caprock oyster(pt.1) was 1.92. The two shells measured from the *Roadcut* (ACR1-Atop-B and ACR1-Ctop-C) had inner leach SIS ages of 5.06Ma (4.80 to 5.28Ma) (see Methods and Supplementary Information for details), and 6.35Ma (6.19 to 6.53Ma), respectively. Additional diagenesis screening techniques on these shells included elemental analysis (see Supplementary Information for details), and variation of ^{87}Sr/^{86}Sr within the leach set of each sample. The results of sample variation compared to the inner leach ^{87}Sr/^{86}Sr are shown in the Supplementary Information, with low Sr isotope variation indicative of better preservation. Samples with low variation tend to exhibit more radiogenic ^{87}Sr/^{86}Sr values. Sample ACR1-Atop-B had a preservation index of 1.56, while ACR1-Ctop-C had a score of 2.33 (see Supplementary Information for details). Based on these screening criteria, we exclude sample ACR1-Ctop-C, which appeared to have been altered by low ^{87}Sr/^{86}Sr fluids (possibly of through leaching of surrounding volcanic material from the Complejo Marifil[37]). The remaining inner leaches that passed screening were averaged by filament to obtain an age of 4.98 +0.245/-0.295Ma (n=6, 2σ S_{EM}) (see Methods and Supplementary Information for details). In the text, this age is reported as a 2σ range, i.e., 4.69-5.23Ma.

Glacial Isostatic Adjustment. To account for changes in vertical displacement and gravity field caused by GIA we use a gravitationally self-consistent sea level model, that accounts for the migration of shorelines and feedback of Earth's rotation axis[57]. We compute both the contribution to GIA from the amount of residual deformation caused by the most recent Pleistocene glacial cycles and from ice age cycles during the Pliocene.

For the first contribution we use the results from Raymo et al.[2], who calculated the residual deformation associated with the ice model ICE-5G[58]. This ice history is paired with a suite of 36 different earth models with varying lithospheric thickness (48km, 71km, and 96km), upper and lower mantle viscosities ($3x10^{20}$ and $5x10^{20}$ Pa s for the upper mantle, and $3x10^{21}$ - $30x10^{21}$ for the lower mantle) to calculate a mean and standard deviation in residual deformation (Figure 5).

For the second contribution we follow the approach described in Dumitru et al.[9] by estimating ice mass variability based on the benthic stack[59]. Following Miller et al.[60] we prescribe that 75% of the benthic $\delta^{18}O$ variability is due to ice volume changes (the rest being due to temperature) and a further scaling of 0.11‰/ 10m to convert $\delta^{18}O_{seawater}$ into ice volume changes. These conversions are highly uncertain[61;62], which highlights the need to obtain local sea level based ice volume estimates. Nonetheless, this scaling was used because it yielded comparable ice volume estimates to the results of Dumitru et al.[9]. To construct an ice history following this ice volume curve we only assume changes in Antarctic ice volume given evidence that continent wide expansion of northern hemisphere ice sheets did only start around 3.3 Ma[63]. However, we acknowledge that an earlier intermittent Greenland ice sheet might have existed[64]. We compute glacial isostatic adjustment using this ice history and the same suite of 36 different earth models described above. We extract local predictions of relative sea level for Argentina, Mallorca, and South Africa. To calculate global mean sea level changes we integrate the amount of water in the ocean basins as a function of time. We next calculate how this quantity has changed relative to the initial state and divide it by the oceanic area calculated at each time.

Note that this setup to calculate the GIA correction deviates slightly from the one described in Dumitru et al.[9] in three small ways, (1) we only consider one GMSL history for the Pliocene rather than a range of histories, (2) we only consider variability in southern hemisphere ice sheets and (3) we calculated GMSL as described above rather than as changes in grounded ice volume.

The GIA corrections from both processes are combined. In a last step we consider the age range for each sea level indicator and average the GIA correction during warm periods, which we define as times that had higher than average sea level over this time period[9]. The mean and standard deviation that is obtained is shown in table 2. We also show the GIA correction calculated in[9] and note that the difference in mean GIA estimates stems mostly from our different definition of global mean sea level. For the analysis in the main text we use the GIA correction described in[9] for the datapoint on Mallorca and not the one recalculated here.

Table 2: GIA correction for Pliocene sea level markers at the three locations discussed in the text. For comparison, we also report the results for Mallorca used in Dumitru et al.[9].

Location	Longitude	Latitude	mean GIA (m)	Stdev GIA (m)
Argentina	65.73° E	44.79° S	-14.6	3.2
South Africa	18.12° W	31.59° S	-9.6	1.6
Mallorca	3.45° W	39.66° N	2.9	2.2
Mallorca[9]	3.45° W	39.66° N	1.3	3.1

Vertical Land Motions. VLMs were extracted from published Dynamic Topography models[44;45] using the Gplates portal (http://portal.gplates.org/). The values extracted are reported in Table 3. Flament et al.[44] focus on the surface expression of subduction dynamics in South America. Their results are based on forward advection modeling with different tectonic surface boundary conditions. The different cases are based on different timings of slab flattening. Müller et al.[45] have a global focus and combine back advection (initialized with a seismic tomography
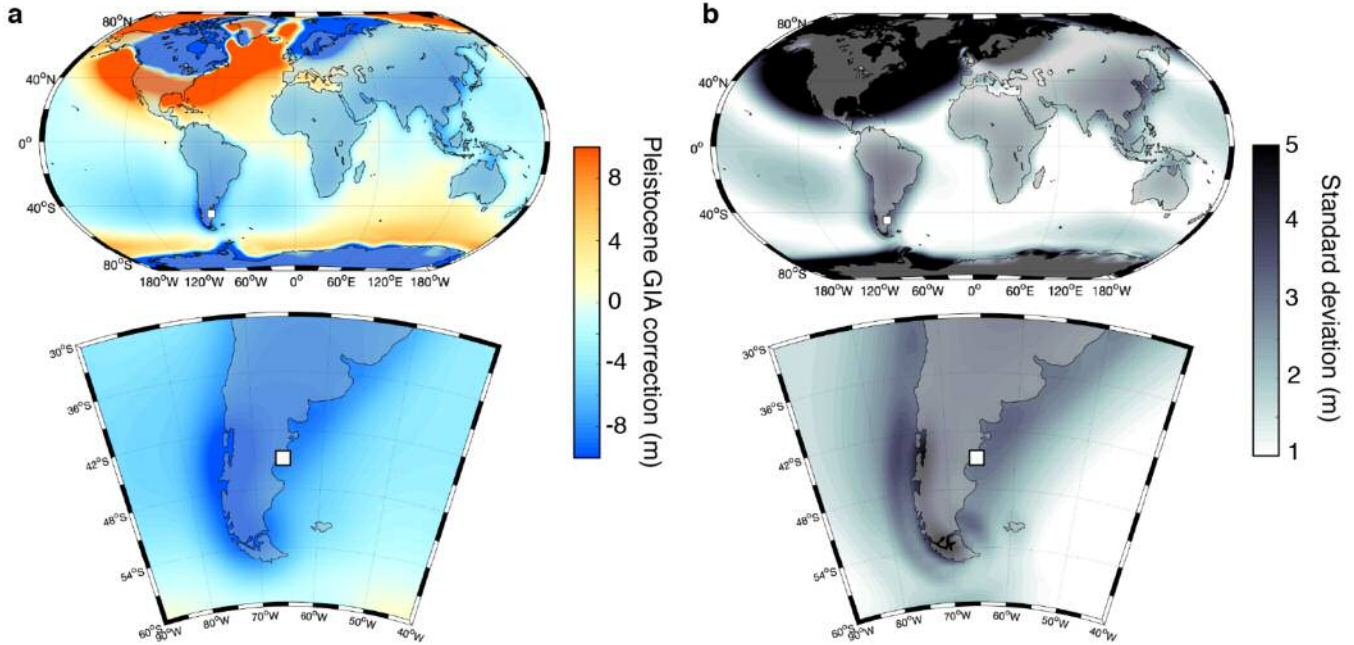
Figure 5: GIA contribution due to ongoing adjustment. The maps show the GIA contribution caused by the incomplete present-day adjustment to the late Pleistocene ice and ocean loading cycles. **a**) Model simulation using a viscosity structure of 5×10^{20} Pa s viscosity in the upper mantle, 5×10^{21} Pa s viscosity in the lower mantle, and an elastic lithospheric thickness of 96 km. **b**) Standard deviation of model predictions obtained using 36 different radial viscosity profiles, including varying the lithospheric thickness. The square in all insets marks the position of Camarones.

model) and forward advection with tectonic surface boundary conditions. Their different models are based on different surface plate reconstructions and different viscosity profiles.

Table 3: Amount of Vertical Land Motion (VLM), timeframe and rates extracted from published dynamic topography models for Camarones.

Reference	Model	VLM (m)	Timing (Ma)	Rate (m/Ma)
Müller et al., 2018[45]	M1	4.6	10	0.46
	M2	66.2	10	6.62
	M3	45.0	10	4.50
	M4	58.0	10	5.80
	M5	45.4	10	4.54
	M6	21.8	10	2.18
	M7	25.5	10	2.55
Flament et al., 2015[44]	Case 1	35.7	5	7.14
	Case 2	37.6	5	7.52
	Case 3	22.9	5	4.58
	Case 4	18.6	5	3.73

Author contributions

AR, MP and SR wrote the MS and supplementary materials, including figures. SR elaborated the stratigraphic description of the Roadcut outcrop. MA provided expertise on the faunal composition of the *Roadcut* and *Caprock* outcrops. MRS performed SIS dating and contributed text on SIS methods and results. JA produced GIA estimates, advised on DT and GMSL calculations, and contributed to the writing of the paper. PJH provided expertise on stratigraphic and geological interpretation on the Camarones outcrops. All authors (except JA) participated in different phases of the field expeditions to Camarones. IC identified the *Caprock* site in the field. MER provided expertise on the paleoclimatic implications of the study. All authors revised the main text and Supplementary Information, and agree with its contents.

References

[1] Rovere, A. *et al.* The analysis of last interglacial (mis 5e) relative sea-level indicators: Reconstructing sea-level in a warmer world. *Earth-Science Reviews* **159**, 404–427 (2016).

[2] Raymo, M. E., Mitrovica, J. X., O'Leary, M. J., DeConto, R. M. & Hearty, P. J. Departures from eustasy in pliocene sea-level records. *Nature Geoscience* **4**, 328–332 (2011).

[3] Austermann, J., Mitrovica, J. X., Huybers, P. & Rovere, A. Detection of a dynamic topography signal in last interglacial sea-level records. *Science Advances* **3**, e1700457 (2017).

[4] Dutton, A. *et al.* Sea-level rise due to polar ice-sheet mass loss during past warm periods. *science* **349**, aaa4019 (2015).

[5] DeConto, R. M. & Pollard, D. Contribution of antarctica to past and future sea-level rise. *Nature* **531**, 591–597 (2016).

[6] Khan, N. S. *et al.* Inception of a global atlas of sea levels since the last glacial maximum. *Quaternary Science Reviews* **220**, 359–371 (2019).

[7] Pedoja, K. *et al.* Coastal staircase sequences reflecting sea-level oscillations and tectonic uplift during the quaternary and neogene. *Earth-Science Reviews* **132**, 13–38 (2014).

[8] Rovere, A. *et al.* The mid-pliocene sea-level conundrum: Glacial isostasy, eustasy and dynamic topography. *Earth and Planetary Science Letters* **387**, 27–33 (2014).

[9] Dumitru, O. A. *et al.* Constraints on global mean sea level during pliocene warmth. *Nature* **574**, 233–236 (2019).

[10] Hearty, P. J. *et al.* Pliocene-pleistocene stratigraphy and sea-level estimates, republic of south africa with implications for a 400 ppmv co2 world. *Paleoceanography and Paleoclimatology* **n/a**, n/a (2020).

[11] USGS. Shuttle radar topography mission (srtm) 1 arc-second global. *US Geological Survey* (2015).

[12] Rohling, E. *et al.* Sea-level and deep-sea-temperature variability over the past 5.3 million years. *Nature* **508**, 477–482 (2014).

[13] Raymo, M. E., Kozdon, R., Evans, D., Lisiecki, L. & Ford, H. L. The accuracy of mid-pliocene δ18o-based ice volume and sea level reconstructions. *Earth-Science Reviews* **177**, 291–302 (2018).

[14] Haywood, A. M. *et al.* Are there pre-quaternary geological analogues for a future greenhouse warming? *Philosophical Transactions of the Royal Society A: Mathematical, Physical and Engineering Sciences* **369**, 933–956 (2011).

[15] Fedorov, A. *et al.* Patterns and mechanisms of early pliocene warmth. *Nature* **496**, 43–49 (2013).

[16] Lunt, D. J. *et al.* Earth system sensitivity inferred from pliocene modelling and data. *Nature Geoscience* **3**, 60–64 (2010).

[17] Grant, G. *et al.* The amplitude and origin of sea-level variability during the pliocene epoch. *Nature* **574**, 237–241 (2019).

[18] Solgaard, A. M., Reeh, N., Japsen, P. & Nielsen, T. Snapshots of the greenland ice sheet configuration in the pliocene to early pleistocene. *Journal of Glaciology* **57**, 871–880 (2011).

[19] Naish, T. *et al.* Obliquity-paced pliocene west antarctic ice sheet oscillations. *Nature* **458**, 322–328 (2009).

[20] Pollard, D. & DeConto, R. M. Modelling west antarctic ice sheet growth and collapse through the past five million years. *Nature* **458**, 329–332 (2009).

[21] Cook, C. P. *et al.* Dynamic behaviour of the east antarctic ice sheet during pliocene warmth. *Nature Geoscience* **6**, 765–769 (2013).

[22] Dolan, A. M. *et al.* Sensitivity of pliocene ice sheets to orbital forcing. *Palaeogeography, Palaeoclimatology, Palaeoecology* **309**, 98–110 (2011).

[23] Thomas, C., Livermore, R. & Pollitz, F. Motion of the scotia sea plates. *Geophysical Journal International* **155**, 789–804 (2003).

[24] Rabassa, J. Late cenozoic glaciations in patagonia and tierra del fuego. *Developments in quaternary sciences* **11**, 151–204 (2008).

[25] Guillaume, B., Martinod, J., Husson, L., Roddaz, M. & Riquelme, R. Neogene uplift of central eastern patagonia: Dynamic response to active spreading ridge subduction? *Tectonics* **28** (2009).

[26] Ton-That, T., Singer, B., Mörner, N.-A. & Rabassa, J. Datación de lavas basálticas por 40ar/39ar y geología glacial de la región del lago buenos aires, provincia de santa cruz, argentina. *Revista de la Asociación Geológica Argentina* **54**, 333–352 (1999).

[27] Darwin, C. *Geological observations on South America: Being the third part of the geology of the voyage of the Beagle, under the command of Capt. Fitzroy, RN during the years 1832 to 1836* (Smith, Elder and Company, 65, Cornhill., 1846).

[28] Schellmann, G. & Radtke, U. Coastal terraces and holocene sea-level changes along the patagonian atlantic coast. *Journal of Coastal Research* 983–996 (2003).

[29] Zanchetta, G. *et al.* Middle-to late-holocene relative sea-level changes at puerto deseado (patagonia, argentina). *The Holocene* **24**, 307–317 (2014).

[30] Pappalardo, M. *et al.* Coastal landscape evolution and sea-level change: A case study from central patagonia (argentina). *Zeitschrift für Geomorphologie* **59**, 145–172 (2015).

[31] Rostami, K., Peltier, W. & Mangini, A. Quaternary marine terraces, sea-level changes and uplift history of patagonia, argentina: comparisons with predictions of the ice-4g (vm2) model of the global process of glacial isostatic adjustment. *Quaternary Science Reviews* **19**, 1495–1525 (2000).

[32] Schellmann, G. & Radtke, U. Esr dating stratigraphically well-constrained marine terraces along the patagonian atlantic coast (argentina). *Quaternary International* **68**, 261–273 (2000).

[33] Rutter, N. *et al.* Correlation and dating of quaternary littoral zones along the patagonian coast, argentina. *Quaternary Science Reviews* **8**, 213–234 (1989).

[34] Del Río, C., Griffin, M., McArthur, J., Martínez, S. & Thirlwall, M. Evidence for early pliocene and late miocene transgressions in southern patagonia (argentina): 87sr/86sr ages of the pectinid" chlamys" actinodes (sowerby). *Journal of South American Earth Sciences* **47** (2013).

[35] Bini, M. *et al.* Mid-holocene relative sea-level changes along atlantic patagonia: new data from camarones, chubut, argentina. *The Holocene* **28**, 56–64 (2018).

[36] Feruglio, E. *Descripción geológica de la Patagonia*, vol. 1 (Impr. y Casa Editora" Coni", 1949).

[37] Lema, H. A. *et al.* Hoja geológica 4566-ii y iv camarones (2001).

[38] Rovere, A. *et al.* Survey data, models and dated samples of the Pliocene shorelines of Camarones, Argentina. (2020). URL https://doi.org/10.5281/zenodo.3929151. Pre-review version.

[39] Piñón, D., Zhang, K., Wu, S. & Cimbaro, S. A new argentinean gravimetric geoid model: Geoidear. In *International Symposium on Earth and Environmental Sciences for Future Generations*, 53–62 (Springer, 2017).

[40] Braun, J. The many surface expressions of mantle dynamics. *Nature Geoscience* **3**, 825–833 (2010).

[41] Moucha, R. *et al.* Dynamic topography and long-term sea-level variations: There is no such thing as a stable continental platform. *Earth and Planetary Science Letters* **271**, 101–108 (2008).

[42] Moucha, R. & Ruetenik, G. A. Interplay between dynamic topography and flexure along the us atlantic passive margin: Insights from landscape evolution modeling. *Global and Planetary Change* **149**, 72–78 (2017).

[43] Ferrier, K. L., Austermann, J., Mitrovica, J. X. & Pico, T. Incorporating sediment compaction into a gravitationally self-consistent model for ice age sea-level change. *Geophysical Journal International* **211**, 663–672 (2017).

[44] Flament, N., Gurnis, M., Müller, R. D., Bower, D. J. & Husson, L. Influence of subduction history on south american topography. *Earth and Planetary Science Letters* **430**, 9–18 (2015).

[45] Müller, R. D., Hassan, R., Gurnis, M., Flament, N. & Williams, S. E. Dynamic topography of passive continental margins and their hinterlands since the Cretaceous. *Gondwana Research* **53**, 225–251 (2018).

[46] Wessel, P. & Smith, W. H. A global, self-consistent, hierarchical, high-resolution shoreline database. *Journal of Geophysical Research: Solid Earth* **101**, 8741–8743 (1996).

[47] Bird, P. An updated digital model of plate boundaries. *Geochemistry, Geophysics, Geosystems* **4** (2003).

[48] Rovere, A. Alerovere/paleo-sl-utilities 1.4 (2020). URL https://doi.org/10.5281/zenodo.3929167.

[49] Shennan, I. Flandrian sea-level changes in the fenland. ii: Tendencies of sea-level movement, altitudinal changes, and local and regional factors. *Journal of Quaternary Science* **1**, 155–179 (1986).

[50] Green, J., Huber, M., Waltham, D., Buzan, J. & Wells, M. Explicitly modelled deep-time tidal dissipation and its implication for lunar history. *Earth and Planetary Science Letters* **461**, 46–53 (2017).

[51] McArthur, J., Howarth, R. & Shields, G. Strontium isotope stratigraphy. *The geologic time scale* **1**, 127–144 (2012).

[52] Bailey, T., McArthur, J., Prince, H. & Thirlwall, M. Dissolution methods for strontium isotope stratigraphy: whole rock analysis. *Chemical Geology* **167**, 313–319 (2000).

[53] Li, D., Shields-Zhou, G. A., Ling, H.-F. & Thirlwall, M. Dissolution methods for strontium isotope stratigraphy: Guidelines for the use of bulk carbonate and phosphorite rocks. *Chemical Geology* **290**, 133–144 (2011).

[54] McArthur, J. M. Recent trends in strontium isotope stratigraphy. *Terra nova* **6**, 331–358 (1994).

[55] Brand, U. & Veizer, J. Chemical diagenesis of a multicomponent carbonate system; 1, trace elements. *Journal of Sedimentary Research* **50**, 1219–1236 (1980).

[56] Gothmann, A. M. *et al.* Fossil corals as an archive of secular variations in seawater chemistry since the mesozoic. *Geochimica et Cosmochimica Acta* **160**, 188–208 (2015).

[57] Kendall, R. A., Mitrovica, J. X. & Milne, G. A. On postglacial sea level–ii. numerical formulation and comparative results on spherically symmetric models. *Geophysical Journal International* **161**, 679–706 (2005).

[58] Peltier, W. Global glacial isostasy and the surface of the ice-age earth: the ice-5g (vm2) model and grace. *Annual Review of Earth and Planetary Sciences* **32**, 111–149 (2004).

[59] Lisiecki, L. E. & Raymo, M. E. A pliocene-pleistocene stack of 57 globally distributed benthic $\delta18o$ records. *Paleoceanography* **20** (2005).

[60] Miller, K. G. *et al.* High tide of the warm pliocene: Implications of global sea level for antarctic deglaciation. *Geology* **40**, 407–410 (2012).

[61] Raymo, M. E., Kozdon, R., Evans, D., Lisiecki, L. & Ford, H. L. The accuracy of mid-pliocene $\delta18o$-based ice volume and sea level reconstructions. *Earth-Science Reviews* **177**, 291–302 (2018).

[62] Gasson, E., DeConto, R. M. & Pollard, D. Modeling the oxygen isotope composition of the antarctic ice sheet and its significance to pliocene sea level. *Geology* **44**, 827–830 (2016).

[63] Jansen, E., Fronval, T., Rack, F. & Channell, J. E. T. Pliocene-pleistocene ice rafting history and cyclicity in the nordic seas during the last 3.5 myr. *Paleoceanography* **15**, 709–721 (2000).

[64] Bierman, P. R., Shakun, J. D., Corbett, L. B., Zimmerman, S. R. & Rood, D. H. A persistent and dynamic east greenland ice sheet over the past 7.5 million years. *Nature* **540**, 256–260 (2016).

Supplementary Information for: An Early Pliocene relative sea level record from Patagonia (Argentina)

Alessio Rovere[1][*], **Marta Pappalardo**[2], **Sebastian Richiano**[3], **Marina Aguirre**[4], **Michael R. Sandstrom**[5], **Paul J. Hearty**[6], **Jacqueline Austermann**[5], **Ignacio Castellanos**[7], and **Maureen E. Raymo**[5]

[1]MARUM - Center for Marine Environmental Sciences, University of Bremen
[2]Department of Earth Sciences, Universitá degli studi di Pisa
[3]Instituto Patagónico de Geología y Paleontología, CONICET, Puerto Madryn
[4]CONICET, CCT-La Plata and Universidad Nacional de La Plata
[5]Lamont Doherty Earth Observatory, Columbia University
[6]Department of Geological Sciences, Jackson School of Geosciences, The University of Texas at Austin
[7]Baker Hughes

Paleo relative sea level indicators in Patagonia

The study of paleo shorelines in Patagonia dates back to Charles Darwin, who was the first to provide an account of the coastal stratigraphy in the region[1]. Nearly a century later, the Italian geologist Feruglio reported the first full account of marine terraces along the Patagonian coast (Chubut and Santa Cruz Provinces)[2], that he grouped into six systems. The two uppermost systems attributed to the to late Pliocene–early Pleistocene[3] based on biostratigrapic features and their high elevation (40-50 and 80-95 m asl). Several studies detailed the stratigraphy, elevation and age of Holocene[4;5], Pleistocene[6;7;8;9;10;11;12] and Pliocene-to-Miocene[13;14] marine and coastal deposits. The Tertiary marine sediments were assigned to Miocene and Pliocene periods mostly on the basis of biostratigraphy. Several authors worked to characterize the Marine Miocene of Patagonia[15;16;17] and the Mio-Pliocene[18]. For which concerns the Early Pliocene, a marine deposit in Northern Patagonia (Rio Negro Province) yielded a fission track age of 4.41 Ma[19], but this age was later considered inconsistent with biostratigraphic characteristics of the deposits and thus rejected[20]. Del Río et al[14] dated samples of mollusks from marine deposits in Central and Southern Patagonia, few hundreds kilometers south of our study area. The marine deposits of Cerro Laciar (300 km south of the area investigated by this study, 170-185m above MSL) yielded ages of 5.10 ± 0.21 Ma, and those of Cañadon Darwin (540 km south of the area investigated by this study, 65-75m above MSL) yielded ages of 5.15 ± 0.18 Ma. These two data points represent the first geochemically constrained evidence of a (Early) Pliocene transgression in the area.

In the coastal area around the Camarones town, the lithology is characterized by a Jurassic volcanic complex (Complejo Marifil), and Upper Paleocene sedimentary rocks (Formación Río Chico)[21]. According to the official geological charts[21], the volcanic complex is composed by reddish rhyolites, leucorhyolites and ignimbrites, whereas the Río Chico formation is made of mudstones, sandstones and conglomerates, often volcaniclastic. Along the same coastal section, fossil beach ridges and marine/beach deposits were recognized from present-day coastline inland.

Holocene. Holocene sea level indicators have been preserved at Camarones as series of proxies marking the maximum sea level transgression and a sequence of regressive beach ridges.

Bini et al., 2018[22] reported precisely measured Holocene RSL proxies dated with ^{14}C, indicating that, between ca. 5300 and 7000 cal. yr BP, RSL was 2 to 4 m above present sea level (elevations referred to the EGM2008 Geoid).

Marine Isotopic Stage 5e. The Last Interglacial is also preserved in the form of relic beach ridges in the Camarones area. These were studied by different authors throughout the years[9;12;10;23], and were dated to MIS 5e using Electron Spin Resonance and U-Series on mollusks (Supplementary Table 1). A recent study by Pappalardo et al. 2015[9] provides more precise measurements, interpretations and additional dating of the MIS 5e beach ridge complex at Camarones. According to these authors, the MIS 5e beach ridges at Camarones were formed in correspondance with a paleo RSL at 7.5 +2/-3.5m above present.

Marine Isotopic Stage 11. At one site south of Camarones town, articulated shells from (Sample Pa 35) was dated by Schellmann and Radtke (2000)[12] as MIS 9 or older. U-series mollusk ages by Pappalardo et al. (2015)[9] confirm the attribution to MIS 11. We measured the deposits dated by these authors at 16.7 ± 0.4m above present sea level.

Detailed description of *Roadcut* and *Caprock* units at Camarones

The *Roadcut* section (Supplementary Figure 1) is characterized by the bedrock (Río Chico formation) outcropping from the road level up to ca.12m above it, mostly sheltered by a tick debris. The topmost part of the bedrock is exposed for a maximum thickness of 1.2m in the western part of the outcrop and it is shaped as a flat, gently eastward (i.e. seaward) dipping platform. All the overlying units are separated from it by a sharp erosional unconformity. Less than 1 km south of the *Roadcut*, another outcrop shows the same geological context. We refer to this as the *Caprock* outcrop (Supplementary Figure 2). This rests on a relative topographic high of the bedrock, which in this point is represented by the volcanic Complejo Marifil, capped by a thin sedimentary unit, as thick as 1m maximum, identical to the upper part of the Cp Unit observed in the *Roadcut* section. Each overlying unit is described separately hereafter.

*correspondence: arovere@marum.de

Table S 1: Ages of beach ridges associated to MIS 5e in the Camarones area.

| Location	Author	Sample	Subsample	Age (ka)	Age uncertainty (ka)	Dating technique
			D2412A	117	21	ESR
Camarones North IV	Schellmann (1998)[23]	Pa 30	D2635	123	22	ESR
			K2412B	139	8	ESR
			D2550	92	9	ESR
		Pa 47c	D2549	99	12	ESR
			D2665	115	9	ESR
Camarones North I	Schellmann (1998)[23]		D2547	117	13	ESR
		Pa 47a	D2546	133	15	ESR
			D2545	137	18	ESR
			D2548	144	19	ESR
			3-0/1	117	5	U-Series
			3-0/2	115	9	U-Series
Camarones 12km South	Rostami et al., 2000[10]	3	3-0/2	110	8	ESR
			3-0/3	112	13	U-Series
			3-0/3	114	9	ESR
		WP64A(3)	N/A	121	0.9	U-Series
Various sites North and south of Camarones	Pappalardo et al., 2015[9]	WP65(1)	N/A	130	2.5	U-Series
		WP68(1)	N/A	131	1.1	U-Series
		WP70(B)	N/A	127	1.2	U-Series

Unit Cm. In the western part of the section on top of the bedrock rests a basal unit (Cm). This is represented by a massive, clast-supported conglomerate with coarse rounded pebbles of different rock types. Pebbles have an imbricated, seaward dipping bedding. Faunal content is absent.

Unit Cp. Eastward, a finer unit (Cp) overlaps the previous one and, towards the East, unconformably rests on the bedrock. Unit Cp is composed of well-cemented fine conglomerates with rounded pebbles, mostly unbroken shells and abundant sandy matrix, displaying a low-angle planar cross-stratification. The uppermost part of Cp contains a dense faunal assemblage in the form of a shellbed, with different shell types (Supplementary Table 2) mostly intact and sometimes with paired valves (articulated), but not in living position. Only the fragmentation of Pectinids is relevant, which is expected even with scarce transport as they have a fragile shell structure. The shells in Unit Cp are characterized by different stages of preservation, depending mostly on the shell type. Big oysters (*Crassostrea* sp.), up to 15 cm in size, are frequent, mostly oriented concordant with strata dip and strike. They underwent partial dissolution, especially of their outer part, which explains the high degree of cementation of this unit. The faunal assemblage of Unit Cp is analogous to that of the Pleistocene terraces towards the coast, with notable exceptions. The absence of *Tegula atra* (cold gastropod species), together with the occurrence of bivalves of warm/warm-temperate affinity (*C. patagonica*, *D. patagonica*, *F. vilardebona*, *M. cf. isabelleana*), is the main difference relative to the Pleistocene deposits. Cp has a maximum thickness of 1m in the western part of the outcrop (stratigraphic column B, Supplementary Figure 1B).

Unit Cs. East of this point, the Cp unit becomes progressively thinner, and is overlapped by a finer unit (Cs) of matrix-supported sandy conglomerates. The contact between Cp and Cs is planar and displays a lateral continuity up to the midpoint of the section, East of which Cs lays directly on the bedrock. The basal part of Cs is massive (Csm) with no sedimentary structures, whereas its uppermost part, separated from Csm by a gradational contact, displays trough cross-stratification (Cst) and, more eastward, longitudinal channels (Csc).

Overall, this section represents the product of sedimentation due to a transgressive event on top of a marine platform carved in the volcanic bedrock. The sequence is fining (and thus deepening) upward. The similarities of the basal unit (Cm) with modern storm berms in the area suggest that it was formed in a backshore environment. We interpret Unit Cp as the product of sedimentation in a foreshore environment. The bedding of marine shells within this unit testifies that they have been re-handled within the surf zone where sediments from upper offshore and shoreface are floated towards the beachface and from there are driven back by rip currents, producing an isorientation of single shells parallel to the current direction. The topmost Units (Csm, Cst and Csc) can be interpreted as mainly developed in middle to upper shoreface. The sedimentary structures within these units can be interpreted as the product of longitudinal currents caused by coastal drift.
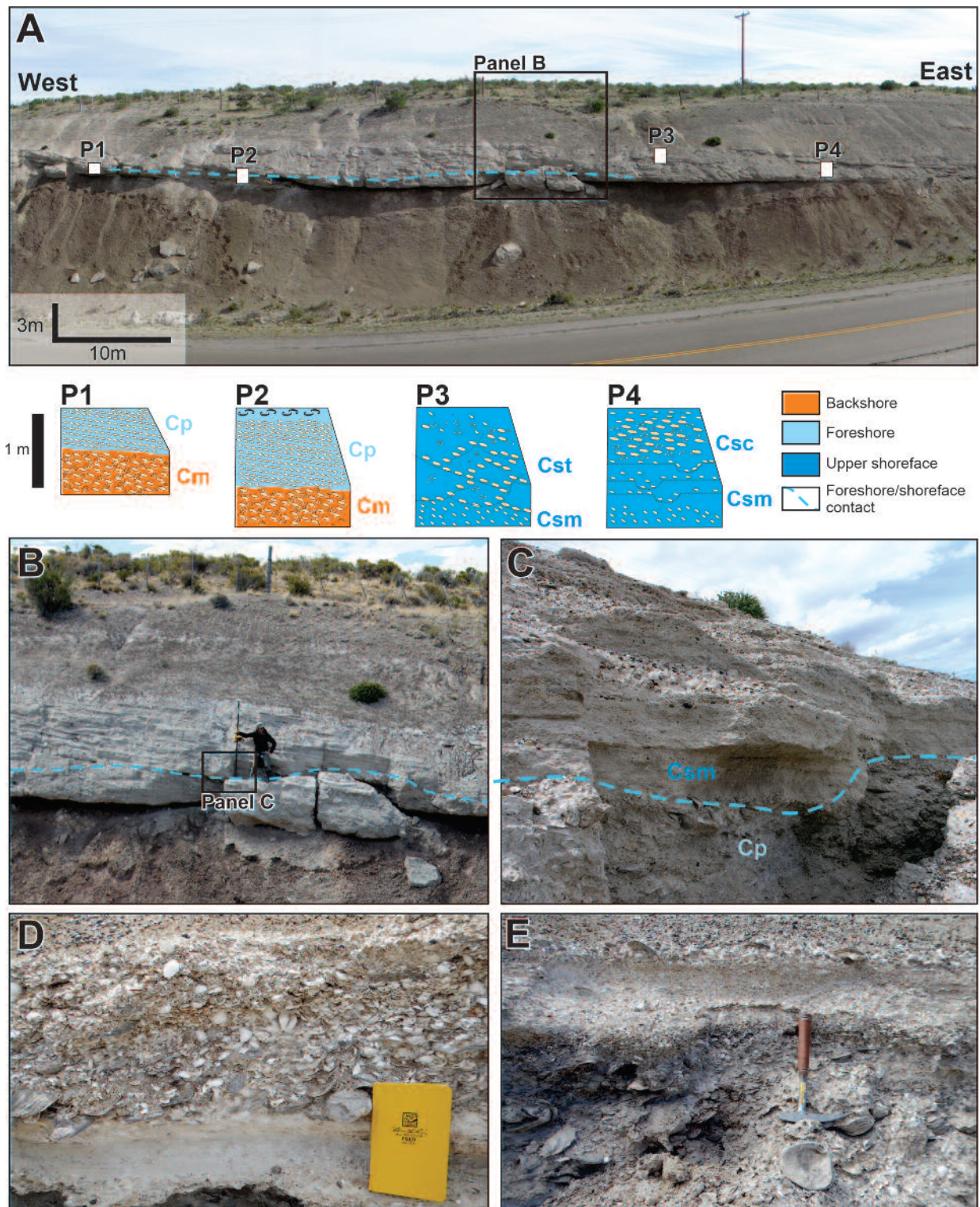
Supplementary Figure 1: A) General view of the *Roadcut* section. Below the photo, four stratigraphic profiles (P1-P4) detailing the relationships between the main sedimentary facies. **Cm**: Conglomerate, massive; **Cp**: Conglomerate with low angle planar cross-stratification; **CSm**: Sandy conglomerate, massive; **CSt**: Sandy conglomerate with trough cross-stratification; **CSc**: Sandy conglomerate with longitudinal channels. B) Location where the elevation of unit **Cp** has been measured (the points listed in the main paper are located near the person standing on the outcrop). C) Detail of the contact between **Cp** (foreshore) and **Csm** (upper foreshore). D) and E) Details of the bivalve-rich horizon sampled for Sr isotopes dating.

Table S 2: Faunal assemblage in the marine deposits outcropping at the *Roadcut* section at Camarones. Most of the species recognized by Feruglio [3;2] and assigned to the highest terrace system (that was tentatively dated to Pliocene) were detected in the Cp Unit of the *Roadcut* section (This work). Nomenclature of the taxa has been updated as some generic or specific names do not agree with those used by Feruglio. * indicates species with warm/warm-temperate affinity.

| **BIVALVIA**	**Feruglio works**	**This work**
Aulacomya atra (Molina, 1782)	X	X
Aequipecten tehuelchus (d'Orbigny, 1842)	X	
Zygochlamys patagonica (King, 1832)	X	X
Pectinidae indet.		X
Ostrea equestris Say, 1834		X
Ostrea puelchana d'Orbigny, 1842	X	
Ostrea tehuelcha Feruglio	X	X
Ostrea cf. tehuelcha Feruglio		X
Ostrea sp		X
Ostrea tehuelcha d'Orbigny*		X
Diplodonta patagonica (d'Orbigny, 1842)*		X
Felaniella vilardeboaena (d'Orbigny, 1846)*	X	
Diplodonta sp	X	
Abra sp		X
Mactra cf. isabellena d'Orbigny, 1846*	X	X
Mactra cf. patagonica d'Orbigny		X
Eurhomalea exalbida (Dilwyn, 1817)		
Ameghinomya antiqua (King, 1832)		X
Pitar rostratus (Philippi, 1844)	X	X
Corbula patagonica d'Orbigny 1845	X	X
GASTROPODA		
Epitonium georgettinum (Kiener, 1838)	X	X
Trophon varians (d'Orbigny, 1841)	X	X
Trophon geversianus (Pallas, 1774)	X	X
Trophon laciniatus (Martin)	X	X
Adelomelon ancilla (Lightfoot, 1786)	X	X
Adelomelon ferussaci (Donovan, 1824)		
Adelomelon sp		X
Odontocymbiola magellanica (Gmelin, 1791)	X	X
Olivancillaria auricularia (Lamarck, 1811)	X	X
Olivancillaria cf. carcellesi Klappenbach, 1965		
Buccinanops deformis (P.P. King, 1832)	X	X
Buccinanops cochlidium (Dilwyn, 1817)	X	
Buccinanops sp	X	X
Siphonaria lessonii Blainville, 1827		
Volutidae indet.	X	X

Supplementary age information.

Details on samples and SIS analyses performed are shown hereafter, in Supplementary Figures 3 to 7. Full SIS age results are reported in Supplementary Table 4.

Initial field selection criteria involved visual assessment based on shell thickness, coloration, and diagnostic features of preservation, including microborings, Fe and Mg staining, fragmentation of original layers, and irregularities in structure [14;24;25] (Supplementary Figure 4 . In the laboratory, samples were slabbed, polished and imaged using an optical microscope with CCD camera for further inspection. and an ASPEX Express scanning electron microscope (SEM). This preliminary screening method helps identify locations of alteration that can be correlated with the $^{87}Sr/^{86}Sr$ leach variations and establishes the overall integrity of preservation in each shell. A preservation scoring system was established as outlined in Hearty et al. (2020)[26], with optical and SEM images assigned scores from "1" (no visible alteration) to "3" (significant alteration observable) based on screening criteria above (Supplementary Table 3).

Shells were micro sampled in the best-preserved regions and homogenized into a fine powder using a dremel drill or acid-cleaned agate mortar and pestle (except for sample ACC1-A pt2, which was kept as a fragment for Sr isotope analysis). Minor and trace elements were measured for three samples on a Thermo iCap Q quadrupole ICP-MS at LDEO. Samples were prepared and analyzed following methods similar to Yu et al[27]. Briefly, ca.250 μg of powder was diluted to 75 ppm Ca (to negate matrix effects), and run alongside calibration standards covering the
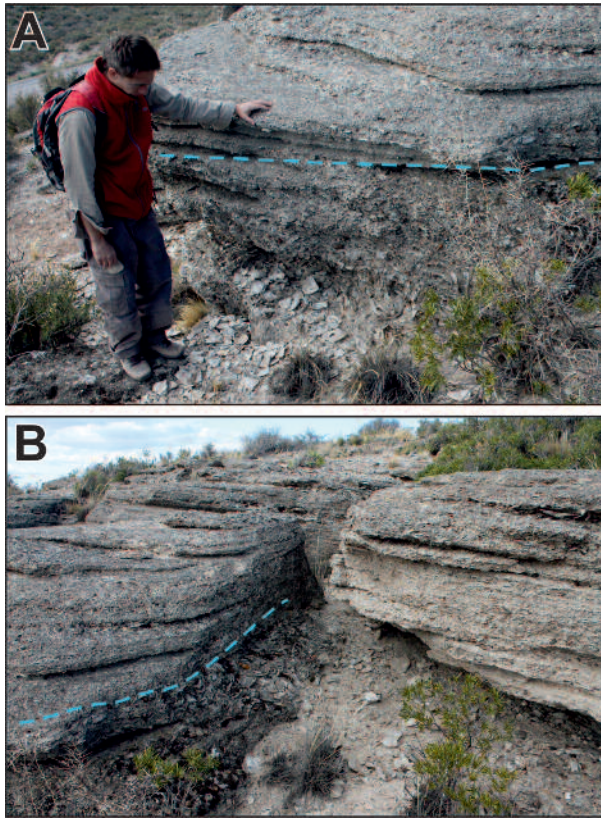
Supplementary Figure 2: A) and B) Contact between the unit Cp (lower) and Cs (higher) at the *Caprock* site.
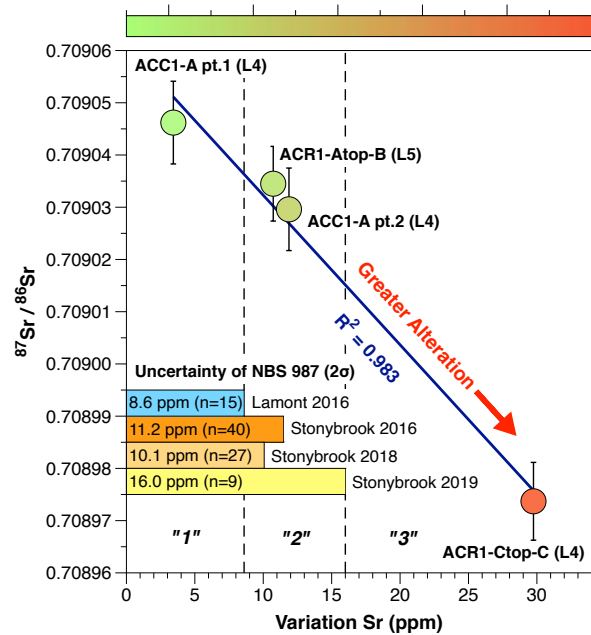

Supplementary Figure 3: Variation of $^{87}Sr/^{86}Sr$ within a leach set (as ppm) vs. the inner leach $^{87}Sr/^{86}Sr$ of that shell. Sr leach variation scores are shown by dashed black line; these scores are based on the range of ppm error from seasonal long-term averages of the standard NBS 987. Green circles have low variation within leach sets (usually better preservation) and display younger SIS ages than shell ACR1-Ctop-C (red point) with high variation. This sample is excluded from the average shoreline SIS age based on high Sr variation and other screening criteria (Supplementary Table 3). Long-term uncertainty of standard NBS987 for each year/lab plotted on lower left as ppm variation.

range of elements concentrations. The results were normalized to the in-house reference standards QC-Calcite and planktonic standard V03, the latter of which has long-term (n = 86) 2σ errors of: Sr/Ca = 1.4%, Mg/Ca = 1.3%, U/Ca = 3.0%, Ba/Ca = 1.8%, Mn/Ca = 1.2%, Al/Ca = 15.8%, Fe/Ca = 2.1% and Na/Ca = 1.3%. A Holocene bivalve (*Tridactna gigas* standard JCt-1) was run alongside the samples for comparison. An elemental scoring system was established for Mg, Mn, and Fe (Supplementary Table 3), elements thought to be indicative of diagenesis[28;29;26]. Scores ranged from "1" (unaltered) to "3" (altered) based on comparison to a set of Holocene corals and bivalves (see Sandstrom et al., in review). Sample splits were taken for Sr isotope analysis (ca. 50 mg for leach fraction, and ca. 10 mg for full dissolution).

Leaching procedures are modified from Bailey et al[30] (see Hearty et al., 2020[26]), and involve weak (ca. 0.1M) Acetic acid leaches on the powdered/fragmented shell, designed to preferentially dissolve the more loosely bound secondary $^{87}Sr/^{86}Sr$ material before attacking the primary Sr. Typically, four to five leaches were performed per sample, each dissolving ca. 12mg (20-25%) of the material, along with one full dissolution of a separate split to average the bulk $^{87}Sr/^{86}Sr$ ratio. Only the initial and inner leaches were measured, along with full dissolution splits (Supplementary Table 4 and Supplementary Figure 5). Sr was isolated and dried down using typical separation techniques with Eichon exchange resin. Following separation, 1% of Sr was removed and measured on a mass spectrometer to determine concentration. A drop of 0.05 N Phosphoric acid was added

and 150-375 ng Sr was loaded onto degassed Rhenium filaments using tantalum chloride loader.

$^{87}Sr/^{86}Sr$ ratios were measured on either an IsotopX Phoenix62 Thermal Ionization Mass Spectrometer (TIMS) at Stonybrook University, or a Finnigan Triton Plus TIMS at Lamont-Doherty Earth Observatory (LDEO). Measurements at Stonybrook were conducted in a very similar manner to Gothmann et al[29], with a dynamic routine measuring masses 84, 85, 86, 87, and 88 over 160 cycles for each sample. Filaments were slowly ramped up to 2.8 - 3.2 A and a temperature of ca. 1400 degrees Celsius, to achieve a beam intensity between 3-5 V on mass 88. TIMS measurements at LDEO were carried out using a static routine for 200-400 cycles with similar parameters to Stonybrook. The Sr isotope external standard NBS SRM 987 long-term instrument accuracy at the two labs was computed every season and ranged between 8.6 - 16 ppm (2σ) (Supplementary Figure 3). At Stonybrook: NBS 987 = 0.7102445 ± 0.0000079 (2σ; 2016, n = 40); 0.7092414 ± 0.0000072 (2σ; 2018, n =27), and 0.7102437 ± 0.0.0000114 (2σ; 2019, n =9) and at LDEO: NBS 987 = 0.7102375 ± 0.0000061 (2σ; 2016, n = 15). Sr isotopes were all corrected for mass fractionation based on an $^{86}Sr/^{88}Sr$ ratio of 0.1194 and normalized to the accepted NBS 987 standard value = 0.709248. Sr isotope stratigraphy ages were calculated using the LOWESS version 5 curve from McArthur et al[28]. Sr

215 isotope variations (in ppm) within leach sets were calculated for
216 each sample (Supplementary Table 3) and a scoring system from
217 "1" to "3" was established based on long-term uncertainties of
218 NBS 987 (see figure S3 and Sandstrom et al.,in review).
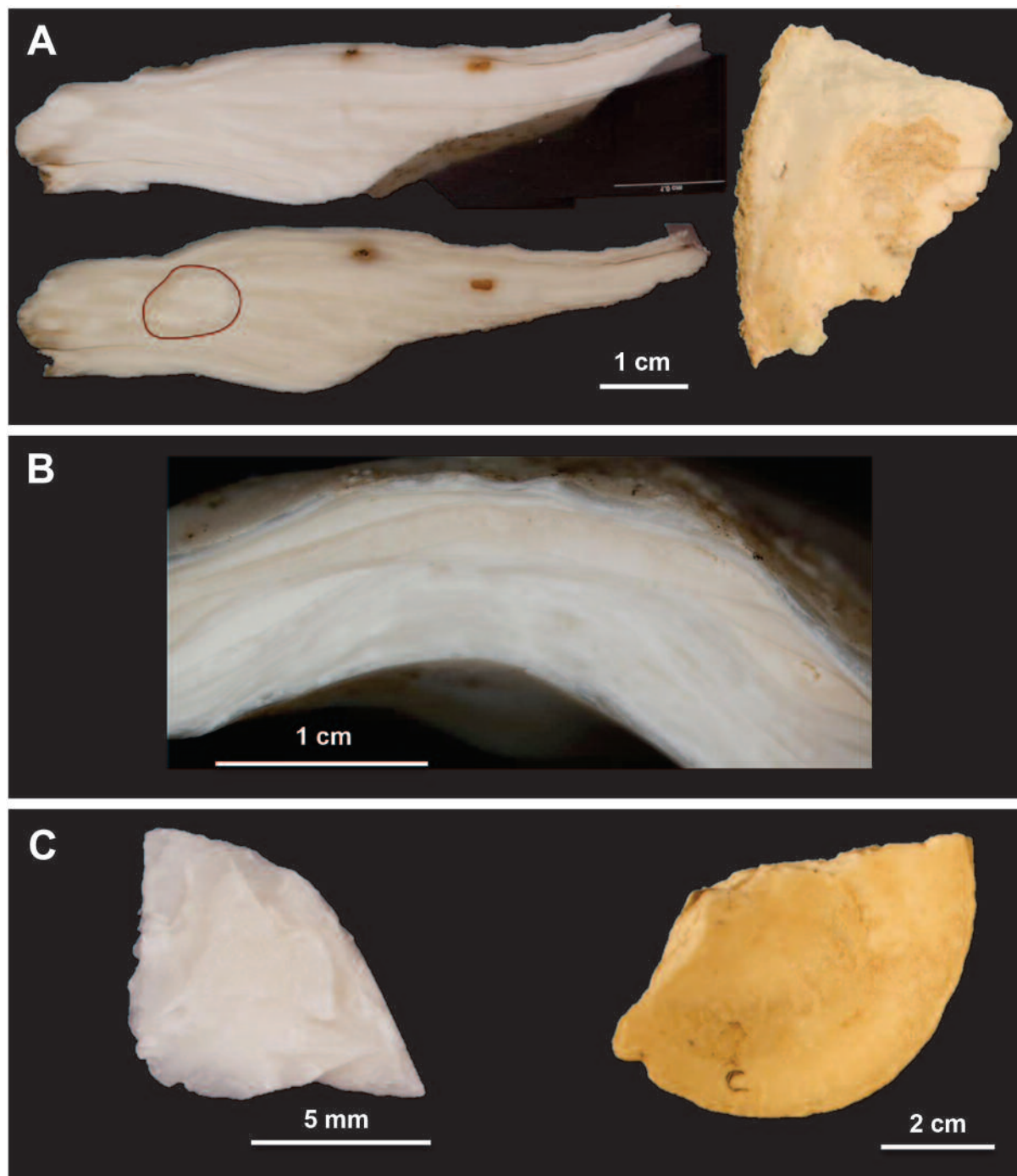
Supplementary Figure 4: Sample images. A) Oyster shell ACC1-A, showing slabbed x-section (top left), part 3 drill location (bottom left), and original shell fragment (right). B) Sample ACR1-Atop-B slabbed x-section. C) Shell ACR1-Ctop-C showing fragment used in Sr isotope dating (left) and partial shell collected from the field (right).
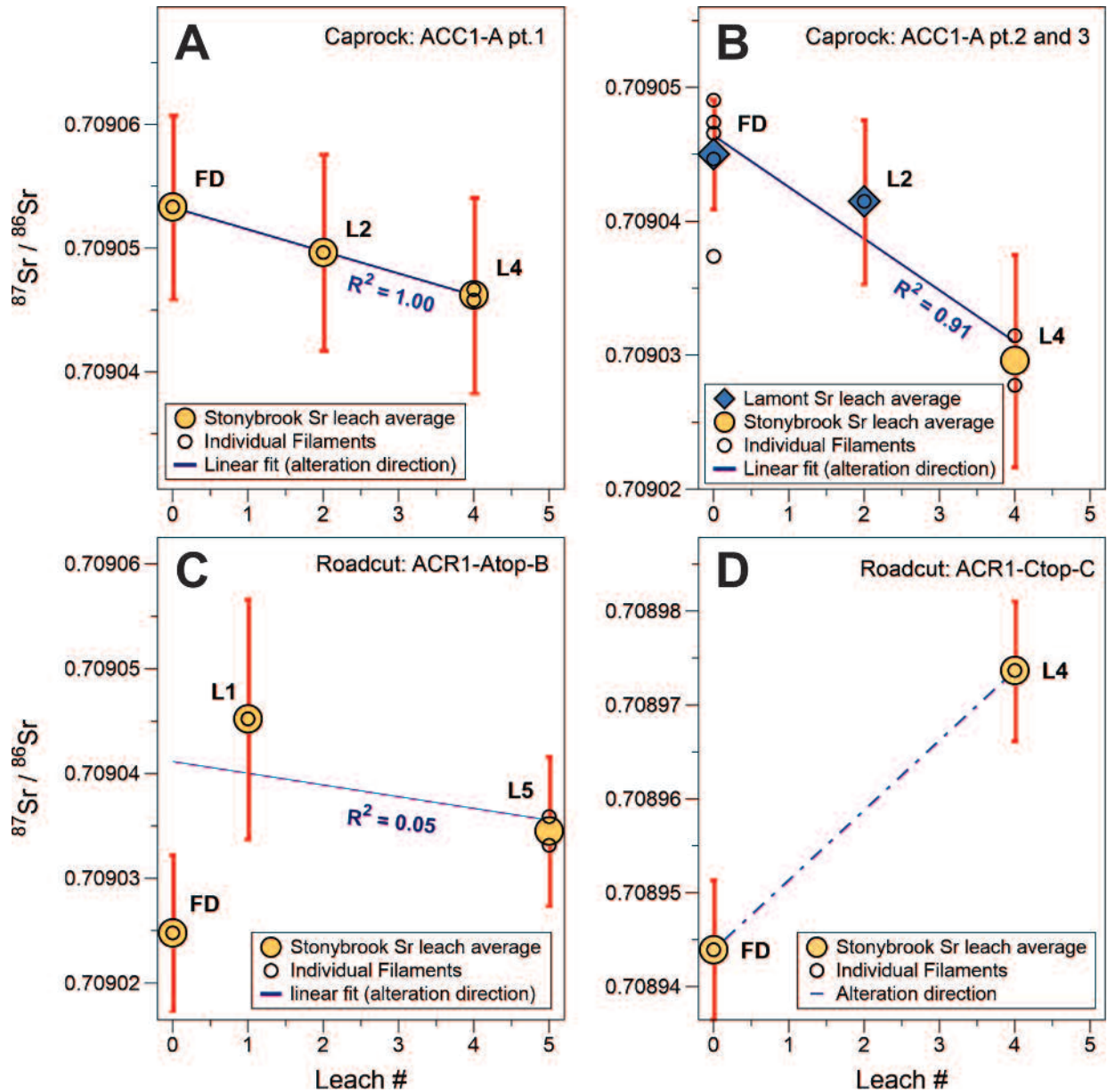
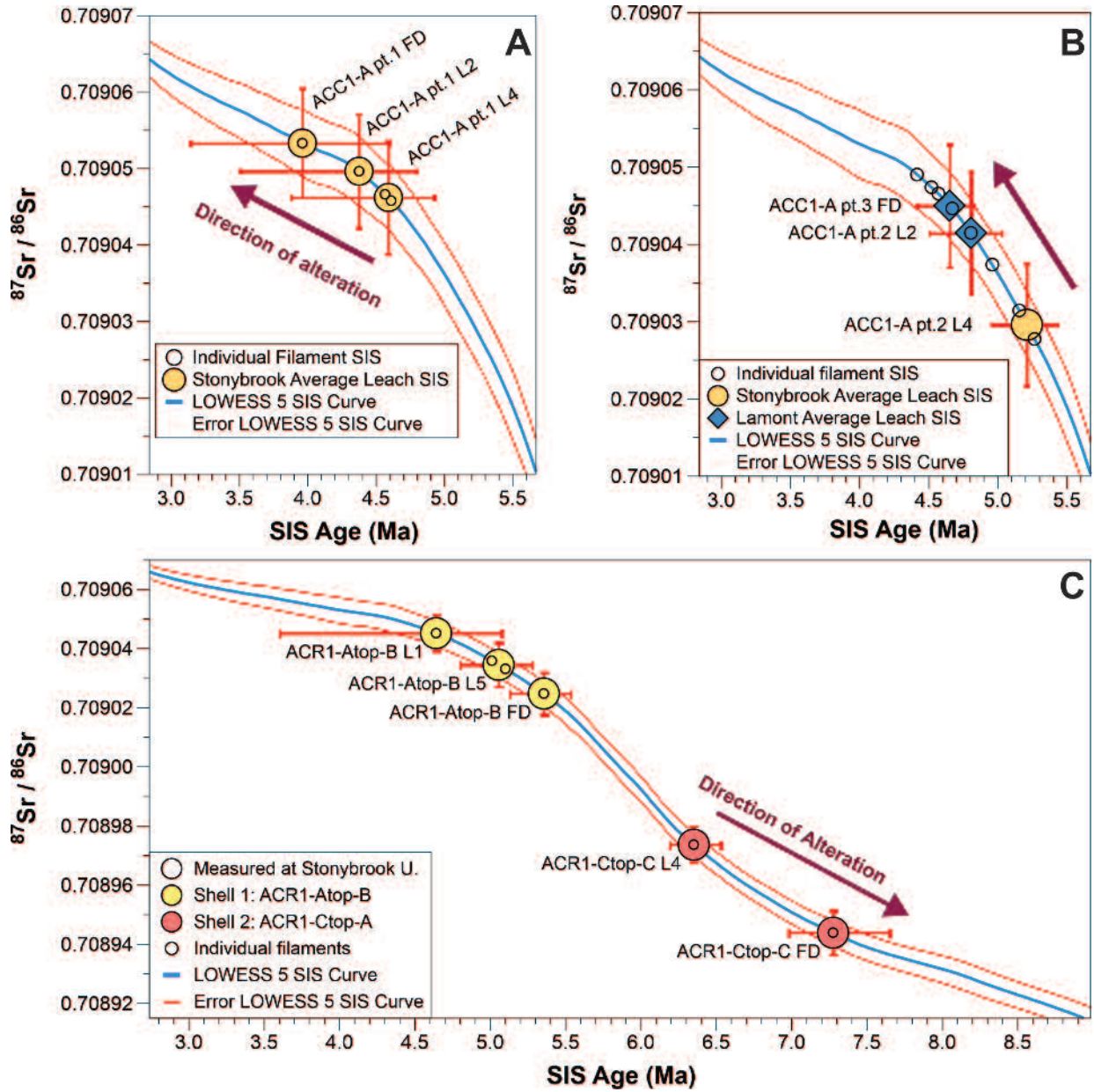Supplementary Figure 5: Sr isotope leach set data for individual sample areas. Red error bars represent 2σ external uncertainty of NBS987 (except for full dissolution ACC1-A pt.3 FD, which is 2σ standard error of the mean). Linear regression lines (blue) indicate direction of alteration, with altering fluids causing the *Caprock* oyster (A and B) to appear slightly younger (more radiogenic $^{87}Sr/^{86}Sr$), and the *Roadcut* samples (C and D) to appear older (alteration fluid with low $^{87}Sr/^{86}Sr$). A and B) Leach set data for sample ACC1-A parts 1 and 2 showing less radioactive $^{87}Sr/^{86}Sr$ (increased SIS age) with better preservation (L4). C) The inner leach lies between the initial leach and full dissolution, overlapping both within uncertainty. The leach set suggests alteration fluids cause ages to appear younger, while the full dissolution indicates the opposite. However, based upon the excellent preservation index score, the inner leach (L5) most likely reflects the original Sr isotopic ratio. D) The trend of significantly increasing $^{87}Sr/^{86}Sr$ of the inner leach compared to the full dissolution indicates post-depositional alteration in this sample.
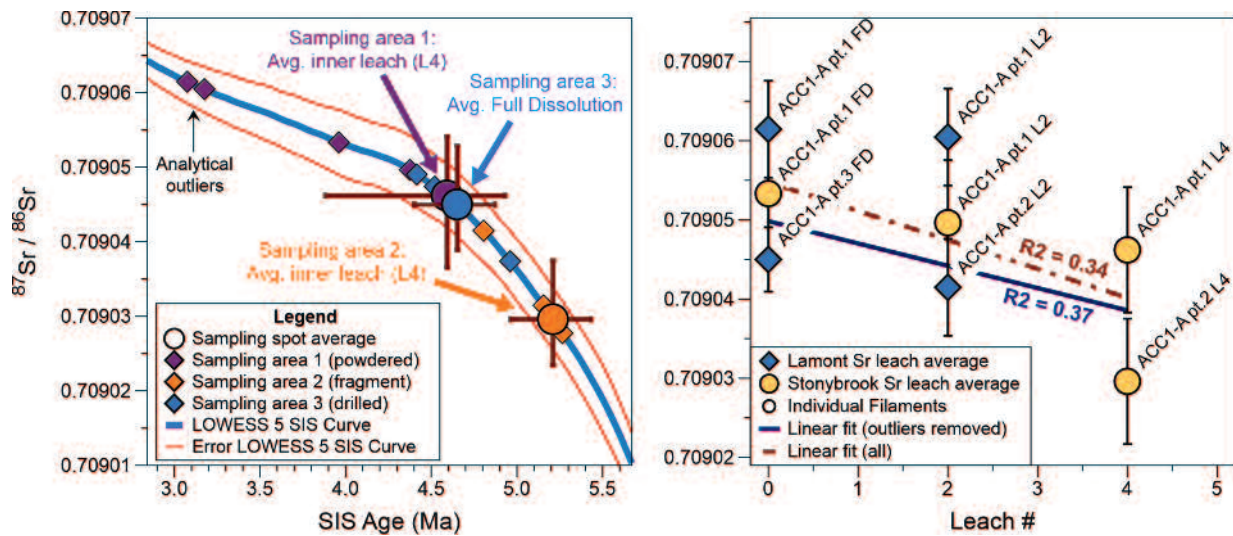
Supplementary Figure 6: Oyster shell ACC1-A (*Caprock*) detailed Sr isotopes and SIS age assignments from three different sampling locations (Left panel). Right panel shows leach Sr values and different TIMS machines (yellow = stonybrook, blue = Lamont). Sample splits ACC-1A pt.1 FD and L2 measured at LDEO appear to be outliers for reasons unknown [possibly turret related? as this was the first turret run?]. Repeated measurements on these same splits at SBU yielded more reliable 87Sr/86Sr values that more closely align with other measurements from different sections of this shell, both at SBU and LDEO. Linear regression was computed for all leach averages (red) and also excluding the two outliers (blue) with similar results. There is a slight trend toward less radiogenic values for the better preserved inner leach measurements.

Supplementary Figure 7: Same data as Supplementary Figure 5. Sr isotope leach set data for individual sample areas, plotted against Lowess5 SIS curve. Red error bars represent 2σ external uncertainty of NBS987 (except for full dissolution ACC1-A pt.3 FD, which is 2σ standard error of the mean). Purple arrows indicate direction of alteration, with altering fluids causing the *Caprock* oyster (A and B) to appear younger (more radioactive $^{87}Sr/^{86}Sr$), and the *Roadcut* samples (C) to appear older (in the case of ACR1-Ctop-C), and possibly younger in the case of ACR1-Atop-A, but no distinct trend can be assigned.

Table S 3: Elemental and diagenetic screening results of oyster samples. BDL = below detection limit. n.a. = not measured. [a] JCt-1 is the Holocene Tridactna standard[31]. [b] Samples used in elemental score average. [c] Full dissolution used for variation calculation, as L1 was not measured. [d] Scoring criteria outlined in Sandstrom et al., in review. [e] See Supp. methods and Hearty et al. (2020)[26]. [f] Leach variation scores: "1"= <8.6ppm; "2" = 8.6 to 16 ppm; "3"= >16 ppm. [g] Samples with preservation index scores $\geq$ "2" are considered altered and excluded.

Sample code	ACC1-A pt.1	ACR1-Atop-B	ACR1-Ctop-C	JCt-1[a]
SESAR ISGN ID	IEMRS006J	IEMRS006L	IEMRS006P	N/A
Description	Caprock - Oyster	Roadcut - Oyster	Roadcut - Oyster	Holocene Tridactna
Na/Ca (mmol/mol)	8.1	9.5	11.7	19.9
Mg/Ca (mmol/mol)[b]	2.9	3.3	4.9	1.2
Al/Ca (μmol/mol)	4.6	BDL	20.4	17.2
Mn/Ca (μmol/mol)[b]	78.8	16.2	1484.7	2.6
Fe/Ca (μmol/mol)[b]	1.7	BDL	144.5	BDL
Sr/Ca (mmol/mol)	0.58	0.85	1.50	1.84
Ba/Ca (μmol/mol)	2.2	2.2	5.9	1.6
U/Ca (nmol/mol)	89.2	107.5	155.2	33.3
number of splits	1	2	1	3
87Sr/86Sr leach variation (ppm)	11.88	10.73	29.75[c]	n.a.
Elemental score (1-3)[d]	1.67	1.67	2.33	1.00
SEM score (1-3)[e]	2	n.d.	2	n.a.
Optical score (1-3)[e]	2	1	2	1
^{87}Sr/^{87}Sr variation score (1-3)[f]	2	2	3	n.a.
Preservation Index Score[g] (average of all scores: 1-3)	**1.92**	**1.56**	**2.33**	**1.00**

Table S 4: [87]Sr/[86]Sr results and Sr isotope stratigraphy ages for Caprock and Roadcut outcrops. [a] Inner leach Sr isotope values for sample; [b] Sample leaches excluded based on analytical or diagenetic criteria; [c] Sample excluded from shoreline age based on significant diagenesis (see Table S3); [d] Uncertainty based on 2σSEM; [e] Sample variation is calculated as the difference between the initial leach [or full dissolution] and last leach, multiplied by one million (ppm); [f] Average of inner leaches on samples that passed screeing criteria: ACC1-A pts. 1 and 2, and ACR1-Atop-B; [g] Uncertainty based on combined analytical [2σSEM] and SIS curve [LOWESS 5] errors.

Sample Name	TIMS Lab	Leach ID	Nb. filaments	[87]Sr/[86]Sr (measured)	[87]Sr/[86]Sr (normalized to NBS97)	2σ external uncertainty	Mean SIS Age (Ma)	Maximum SIS Age (Ma)	Minimum SIS Age (Ma)	Uncorrected SIS Age (Ma)
				Average [87]Sr/[86]Sr by Leach						
Caprock										
ACC1-A pt.1 FD	SBU	FD	1	0.7090465	0.7090533	0.0000075	3.960	4.605	3.140	4.58
ACC1-A pt.1 L2	SBU	L2	1	0.7090462	0.7090496	0.0000079	4.375	4.795	3.505	4.59
ACC1-A pt.1 L4 [a]	SBU	L4	2	0.7090427	0.7090462	0.0000079	4.590	4.925	3.880	4.76
ACC1-A pt.1 FD [b]	LDEO	FD	1	0.7090509	0.7090615	0.0000061	3.075	3.745	2.635	4.27
ACC1-A pt.1 L2 [b]	LDEO	L2	1	0.7090499	0.7090605	0.0000061	3.175	3.855	2.695	4.36
ACC1-A pt.2 L2	LDEO	L2	1	0.7090309	0.7090415	0.0000061	4.805	5.030	4.505	5.17
ACC1-A pt.2 L4 [a]	SBU	L4	2	0.7090261	0.7090296	0.0000079	5.210	5.435	4.955	5.32
ACC1-A pt.3 FD	LDEO	FD	5	0.7090345	0.7090344	0.0000041 [d]	4.650	4.415	4.830	5.055
Roadcut										
ACR1-Atop-B FD	SBU	FD	1	0.7090180	0.7090248	0.0000075	5.355	5.535	5.130	5.52
ACR1-Atop-B L1	SBU	L1	1	0.7090409	0.7090452	0.0000114	4.640	5.075	3.605	4.83
ACR1-Atop-B L5 [a]	SBU	L5	2	0.7090279	0.7090345	0.0000072	5.055	5.280	4.800	5.27
ACR1-Ctop-C FD	SBU	FD	1	0.7089371	0.7089439	0.0000075	7.275	7.650	6.980	7.62
ACR1-Ctop-C L4 [a,c]	SBU	L4	1	0.7089668	0.7089737	0.0000075	6.350	6.530	6.190	6.52
Average Shoreline SIS Age										
Average of screened inner leaches [f]	SBU	L4, L5	6	0.7090322	0.7090368	0.0000064 [d]	4.98	5.225 [g]	4.685 [g]	5.13

References

[1] Darwin, C. *Geological observations on South America: Being the third part of the geology of the voyage of the Beagle, under the command of Capt. Fitzroy, RN during the years 1832 to 1836* (Smith, Elder and Company, 65, Cornhill., 1846).

[2] Feruglio, E. *I terrazzi marini della Patagonia* (Cooperativa Tip. Edit. Paolo Galeati, 1933).

[3] Feruglio, E. *Descripción geológica de la Patagonia*, vol. 1 (Impr. y Casa Editora" Coni", 1949).

[4] Schellmann, G. & Radtke, U. Coastal terraces and holocene sea-level changes along the patagonian atlantic coast. *Journal of Coastal Research* 983–996 (2003).

[5] Zanchetta, G. *et al.* Middle-to late-holocene relative sea-level changes at puerto deseado (patagonia, argentina). *The Holocene* **24**, 307–317 (2014).

[6] Bini, M. *et al.* Markers of palaeo sea-level in rocky coasts of patagonia (argentina). *Rendiconti Online della Società Geologica Italiana* **20**, 10–14 (2013).

[7] Fucks, E. *et al.* Influence of quaternary sea level changes in the littoral of chubut, argentina. *Journal of South American Earth Sciences* **88**, 589–598 (2018).

[8] Pappalardo, M. *et al.* Challenges in relative sea-level change assessment highlighted through a case study: The central coast of atlantic patagonia. *Global and Planetary Change* **182**, 103008 (2019).

[9] Pappalardo, M. *et al.* Coastal landscape evolution and sea-level change: A case study from central patagonia (argentina). *Zeitschrift für Geomorphologie* **59**, 145–172 (2015).

[10] Rostami, K., Peltier, W. & Mangini, A. Quaternary marine terraces, sea-level changes and uplift history of patagonia, argentina: comparisons with predictions of the ice-4g (vm2) model of the global process of glacial isostatic adjustment. *Quaternary Science Reviews* **19**, 1495–1525 (2000).

[11] Pedoja, K. *et al.* Uplift of quaternary shorelines in eastern patagonia: Darwin revisited. *Geomorphology* **127**, 121–142 (2011).

[12] Schellmann, G. & Radtke, U. Esr dating stratigraphically well-constrained marine terraces along the patagonian atlantic coast (argentina). *Quaternary International* **68**, 261–273 (2000).

[13] Rutter, N. *et al.* Correlation and dating of quaternary littoral zones along the patagonian coast, argentina. *Quaternary Science Reviews* **8**, 213–234 (1989).

[14] Del Río, C., Griffin, M., McArthur, J., Martínez, S. & Thirlwall, M. Evidence for early pliocene and late miocene transgressions in southern patagonia (argentina): 87sr/86sr ages of the pectinid" chlamys" actinodes (sowerby). *Journal of South American Earth Sciences* **47** (2013).

[15] del Río, C. J., Martínez, S. A. & Scasso, R. A. Nature and origin of spectacular marine miocene shell beds of northeastern patagonia (argentina): Paleoecological and bathymetric significance. *Palaios* **16**, 3–25 (2001).

[16] Dozo, M. T. *et al.* Late miocene continental biota in northeastern patagonia (península valdés, chubut, argentina). *Palaeogeography, Palaeoclimatology, Palaeoecology* **297**, 100–109 (2010).

[17] Farinati, E. & Zavala, C. Trace fossils on shelly substrate. an example from the miocene of patagonia, argentina. *Acta Geologica Hispanica* **37**, 29–36 (2002).

[18] del Río, C. J. Tertiary marine molluscan assemblages of eastern patagonia (argentina): a biostratigraphic analysis. *Journal of Paleontology* **78**, 1097–1122 (2004).

[19] Bigazzi, G., Bonadonna, F., Leone, G. & Zanchetta, G. Primeros datos geoquimicos y geocronologicos a partir de algunas cineritas del area bonarense (1995).

[20] Farinati, E. A. & Zavala, C. A. Asociaciones de megafósiles de invertebrados en el neógeno atlántico de la patagonia argentina (2005).

[21] Lema, H. A. *et al.* Hoja geológica 4566-ii y iv camarones (2001).

[22] Bini, M. *et al.* Mid-holocene relative sea-level changes along atlantic patagonia: new data from camarones, chubut, argentina. *The Holocene* **28**, 56–64 (2018).

[23] Schellmann, G. *Jungkänozoische Landschaftsgeschichte Patagoniens (Argentinien): andine Vorlandvergletscherungen, Talentwicklung und marine Terrassen* (1. Auflage, Essen: Klartext, 1998, 1998).

[24] McArthur, J. M. Recent trends in strontium isotope stratigraphy. *Terra nova* **6**, 331–358 (1994).

[25] Cochran, J. K. *et al.* Effect of diagenesis on the sr, o, and c isotope composition of late cretaceous mollusks from the western interior seaway of north america. *American Journal of Science* **310**, 69–88 (2010).

[26] Hearty, P. J. *et al.* Pliocene-pleistocene stratigraphy and sea-level estimates, republic of south africa with implications for a 400 ppmv co2 world. *Paleoceanography and Paleoclimatology* **n/a**, n/a (2020).

[27] Yu, J., Day, J., Greaves, M. & Elderfield, H. Determination of multiple element/calcium ratios in foraminiferal calcite by quadrupole icp-ms. *Geochemistry, Geophysics, Geosystems* **6** (2005).

[28] McArthur, J., Howarth, R. & Shields, G. Strontium isotope stratigraphy. *The geologic time scale* **1**, 127–144 (2012).

[29] Gothmann, A. M. *et al.* Fossil corals as an archive of secular variations in seawater chemistry since the mesozoic. *Geochimica et Cosmochimica Acta* **160**, 188–208 (2015).

[30] Bailey, T., McArthur, J., Prince, H. & Thirlwall, M. Dissolution methods for strontium isotope stratigraphy: whole rock analysis. *Chemical Geology* **167**, 313–319 (2000).

[31] Watanabe, T., Suzuki, A., Kawahata, H., Kan, H. & Ogawa, S. A 60-year isotopic record from a mid-holocene fossil giant clam (tridacna gigas) in the ryukyu islands: physiological and paleoclimatic implications. *Palaeogeography, Palaeoclimatology, Palaeoecology* **212**, 343–354 (2004).